

Journal of Biophotonics

Indocyanine Green labeling for optical and photoacoustic imaging of Mesenchymal Stem Cells after in vivo transplantation.

--Manuscript Draft--

Manuscript Number:	
Full Title:	Indocyanine Green labeling for optical and photoacoustic imaging of Mesenchymal Stem Cells after in vivo transplantation.
Article Type:	Full Article
Section/Category:	
Keywords:	Photoacoustic imaging; Cell tracking; Indocyanine Green; stem cells; Near Infrared Fluorescence Imaging.
Corresponding Author:	Miriam Filippi University of Torino Torino, Torino ITALY
Corresponding Author Secondary Information:	
Corresponding Author's Institution:	University of Torino
Corresponding Author's Secondary Institution:	
First Author:	Miriam Filippi
First Author Secondary Information:	
Order of Authors:	Miriam Filippi Francesca Garello Francesca Arena Chiara Pasquino Pierangela Giustetto Federica Antico Enzo Terreno
Order of Authors Secondary Information:	
Abstract:	<p>The transplantation of Mesenchymal Stem Cells (MSCs) holds great promise for the treatment of a plethora of human diseases, but new non-invasive procedures are needed to monitor the cell fate in vivo. Already largely used in medical diagnostics, the fluorescent dye Indocyanine Green (ICG) is an established dye to track limited numbers of cells by optical imaging, but it can be visualized also by Photoacoustic Imaging (PAI), which provides a higher spatial resolution than pure near infrared fluorescence imaging (NIRF). Because of its successful use in clinical and preclinical examinations, we chose ICG as PAI cell labeling agent. Optimal incubation conditions were defined for an efficient and clinically translatable MSC labeling protocol, such that no cytotoxicity or alterations of the phenotypic profile were observed, and a consistent intracellular uptake of the molecule was achieved. Suspensions of ICG-labeled cells were both optically and optoacoustically detected in vitro, revealing a certain variability in the photoacoustic spectra. Intramuscular engraftments of ICG-labeled MSCs were clearly visualized by both PAI and NIRF over few days after transplantation in the hindlimb of healthy mice, suggesting that the proposed technique retains a considerable potential in the field of transplantation-focused research and therapy.</p>
Additional Information:	
Question	Response
Please submit a plain text version of your	January 14th, 2018

cover letter here.

Please note, if you are submitting a revision of your manuscript, there is an opportunity for you to provide your responses to the reviewers later; please do not add them to the cover letter.

Dear Editor,

we are submitting the manuscript entitled 'Indocyanine Green labeling for optical and photoacoustic imaging of Mesenchymal Stem Cells after in vivo transplantation', that reports on the use of the clinically approved fluorescent dye Indocyanine Green (ICG) as labeling agent for the visualization of Mesenchymal Stem Cells (MSCs) by both Photoacoustic and Fluorescence-based Imaging.

The present study was carried out at multiple levels, ranging from the in vitro characterization of the technique to the in vivo applicative proof. Its novelty and significance can be summarised as follows:

- 1)The choice of ICG as a safer alternative to conventional photoacoustic nano-sized probes endows the protocol with maximized safety, thus increasing the potential for clinical translatability. The optimal labeling conditions were determined, by identifying the maximum exposure time to the agent that do not alter the viability, proliferation, and marker profile of cells after incubation.
- 2)In these conditions, a good internalization was obtained, such that efficient optical and photoacoustic imaging of cell suspensions in vitro was feasible, allowing to study the PA spectral properties of ICG.
- 3)Intramuscular engraftments composed of limited numbers (3.0×10^5) of labeled MSCs were successfully detected and monitored over time in vivo by both imaging modalities, revealing considerable values of local contrast enhancement in the engraftment site, persisting for days after cell deposition.
- 4)Even though the Fluorescence-based imaging of several types of ICG-labeled cells was already reported (S. E. Boddington, et al., 2010; V. Sabapathy, et al., 2015), our report shows its fundamental role in integrating the photoacoustic information.
- 5)The photoacoustic imaging allowed the video recording of the cell deposition into the tissue during the transplantation, as well as the three-dimensional representation of the engraftments, highlighting the potential utility of the technique in facilitating the collection of data with real-time content and the characterization of the cell engraftments.

Successful preclinical studies fuelled an increasing interest for therapeutic interventions based on the transplantation of stem and progenitor cells, capable of stimulating repair and regeneration of damaged tissue in several diseases affecting the cardiovascular, central nervous, and musculoskeletal system. As the photoacoustic imaging could provide good endogenous contrast among soft tissues and improved spatial resolution with respect to pure optical detection of ICG, in our opinion this efficient, safe and simple labeling technique retains a considerable potential in the field of transplantation-focused research and therapy, possibly being relevant for the future development of new strategies for the cell fate surveillance. As such, we believe this contribution may be of interest to a broader readership.

Yours sincerely,
Enzo Terreno

Indocyanine Green labeling for optical and photoacoustic imaging of Mesenchymal Stem Cells after *in vivo* transplantation.

Filippi M.^{1#} and Garelo F.^{1#}, Arena F.¹, Pasquino C.², Giustetto P.¹, Antico F.², Terreno E.^{1*}

[#] These authors contributed equally to this work

¹ Molecular and Preclinical Imaging Centers, Department of Molecular Biotechnology and Health Sciences, University of Turin, Via Nizza 52, 10126 Torino, Italy.

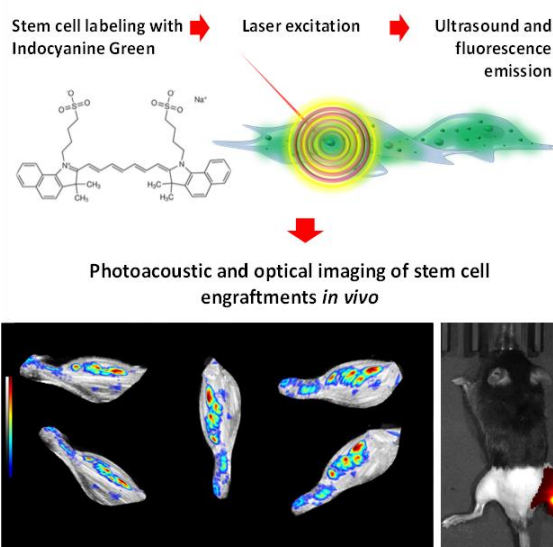
² Department of Molecular Biotechnology and Health Sciences, University of Turin, Via Nizza 52, 10126 Torino, Italy.

Received zzz, revised zzz, accepted zzz

Published online zzz

Key words: Photoacoustic Imaging; Cell tracking; Indocyanine Green; Stem Cells; Near Infrared Fluorescence Imaging.

The transplantation of Mesenchymal Stem Cells (MSCs) holds great promise for the treatment of a plethora of human diseases, but new non-invasive procedures are needed to monitor the cell fate *in vivo*. Already largely used in medical diagnostics, the fluorescent dye Indocyanine Green (ICG) is an established dye to track limited numbers of cells by optical imaging, but it can be visualized also by Photoacoustic Imaging (PAI), which provides a higher spatial resolution than pure near infrared fluorescence imaging (NIRF). Because of its successful use in clinical and preclinical examinations, we chose ICG as PAI cell labeling agent. Optimal incubation conditions were defined for an efficient and clinically translatable MSC labeling protocol, such that no cytotoxicity or alterations of the phenotypic profile were observed, and a consistent intracellular uptake of the molecule was achieved. Suspensions of ICG-labeled cells were both optically and photoacoustically detected *in vitro*, revealing a certain variability in the photoacoustic spectra acquired by varying the excitation wavelength from 680 to 970 nm. Intramuscular engraftments of ICG-labeled MSCs were clearly visualized by both PAI and NIRF over few days after transplantation in the hindlimb of healthy mice, suggesting that the proposed technique retains a considerable potential in the field of transplantation-focused research and therapy.



Stem cells were labeled with the FDA approved fluorescent dye Indocyanine Green (ICG), and detected by both photoacoustic and optical imaging, enabling to monitor the cell fate safely, in dual modality, and with good sensitivity and improved spatial resolution.

1. Introduction

Cell transplantation is an essential tool for biomedical research and a promising approach to achieve curative benefits in several pathologic scenarios.¹ Specifically, due to their major role in regenerative therapies, treatment of immune disorders, and tissue repair, Mesenchymal Stem Cells (MSCs) are commonly involved in cell transplantation-based applications.[1-3] However, these

strategies are not regarded as a first-line therapy yet, mainly because of the limited efficacy shown in several clinical studies.[1,4-5] Since the poor results are very often related to the lack of available information about the cell destiny after transplantation,[4-5] a growing interest has been dedicated to the development of innovative imaging procedures for non-invasive surveillance of the cell fate *in vivo*. [5-6] When the transplantation is performed into superficial tissues, also the imaging techniques with limited penetration depth can be

* Corresponding author: e-mail: enzo.terreno@unito.it, Phone: +39-0116706452, Fax: +39-0116706478

1
2 successfully employed to monitor the cell engraftment
3 and the local biological reaction to the therapy.[7-11]
4 Both Optical Imaging (OI) and Ultrasonic Imaging (US)
5 suffer from wave scattering into living tissue, but display
6 other complementary properties.[12-13] Near Infrared
7 Fluorescence (NIRF) imaging is one of the most used OI
8 modalities and it is endowed with elevated sensitivity, but
9 lacks spatial resolution. On the other side, US imaging
10 provides a satisfactory sub-mm spatial resolution at
11 centimeters depth and intermediate sensitivity.[14]
12 Photoacoustic Imaging (PAI) merges the advantages of
13 the two techniques and compensates their limitations, thus
14 paving the way towards new imaging applicative
15 horizons.[12-13] So far, PA cell imaging has been mostly
16 performed by loading cells with gold and carbon-based
17 nano-objects,[15-18] offering a considerable efficiency in
18 contrast detection, but with documented episodes of
19 cytotoxicity and adverse immune reactions.[16,19-20]
20 However, also small molecules (either fluorescence
21 quenchers or low quantum-yield emitters) display
22 properties of interaction with the electromagnetic
23 radiation leading to photothermal conversion and ultrasonic
24 emission.[21] Among fluorescent compounds, we chose
25 Indocyanine Green dye (ICG), a tricyanocyanine dye that,
26 when dissolved in aqueous solution in the micromolar
27 range, exhibits absorbance and emission peaks at 780 nm
28 and 830 nm, respectively.[22-23] Since its FDA approval
29 for human use in 1959,[22] this molecule has been
30 clinically employed for a myriad of medical purposes,
31 including phototherapy, ophthalmic angiography,
32 laparoscopy, hepatic function and cardiac output
33 determination, sentinel lymph node detection in oncology,
34 vascular and brain surgery, and several others.[22-27]
35 With a fluorescence quantum yield of about 10% in water,
36 ICG can non-radiatively release $\approx 90\%$ of its excited
37 energy in the form of heat,[28] thus becoming a popular
38 option for the surface functionalization of particles
39 detectable by both NIRF and PAI.[15,21] ICG has already
40 been proposed as cell labeling agent in cell tracking by
41 NIRF,[29-30] but it has never been envisaged for the
42 photoacoustic cell visualization in its molecular form.
43 Besides retaining superior imaging potential than pure
44 NIRF, PAI of cells loaded with ICG would also offer a
45 safer labeling route than current standard probes.
46 Therefore, in the present study, this dye was selected as
47 dual fluorescence and optoacoustic cell tracer to label
48 murine bone marrow-derived MSCs. After having defined
49 the optimal labeling conditions, the characteristics and
50 persistence of NIRF and PA signals were monitored either
51 in *in vitro* cell suspensions or *in vivo* engraftments
52 obtained by intramuscular transplantation in healthy mice.
53

54 2. Experimental

55 2.1 Animal Care and Use

56
57
58
59
60
61
62
63
64
65
66
67
68
69
70
71
72
73
74
75
76
77
78
79
80
81
82
83
84
85
86
87
88
89
90
91
92
93
94
95
96
97
98
99
100
101
102
103
104
105
106
107
108
109
110
111
112
113
114
115
116
117
118
119
120
121
122
123
124
125
126
127
128
129
130
131
132
133
134
135
136
137
138
139
140
141
142
143
144
145
146
147
148
149
150
151
152
153
154
155
156
157
158
159
160
161
162
163
164
165
166
167
168
169
170
171
172
173
174
175
176
177
178
179
180
181
182
183
184
185
186
187
188
189
190
191
192
193
194
195
196
197
198
199
200
201
202
203
204
205
206
207
208
209
210
211
212
213
214
215
216
217
218
219
220
221
222
223
224
225
226
227
228
229
230
231
232
233
234
235
236
237
238
239
240
241
242
243
244
245
246
247
248
249
250
251
252
253
254
255
256
257
258
259
260
261
262
263
264
265
266
267
268
269
270
271
272
273
274
275
276
277
278
279
280
281
282
283
284
285
286
287
288
289
290
291
292
293
294
295
296
297
298
299
300
301
302
303
304
305
306
307
308
309
310
311
312
313
314
315
316
317
318
319
320
321
322
323
324
325
326
327
328
329
330
331
332
333
334
335
336
337
338
339
340
341
342
343
344
345
346
347
348
349
350
351
352
353
354
355
356
357
358
359
360
361
362
363
364
365
366
367
368
369
370
371
372
373
374
375
376
377
378
379
380
381
382
383
384
385
386
387
388
389
390
391
392
393
394
395
396
397
398
399
400
401
402
403
404
405
406
407
408
409
410
411
412
413
414
415
416
417
418
419
420
421
422
423
424
425
426
427
428
429
430
431
432
433
434
435
436
437
438
439
440
441
442
443
444
445
446
447
448
449
450
451
452
453
454
455
456
457
458
459
460
461
462
463
464
465
466
467
468
469
470
471
472
473
474
475
476
477
478
479
480
481
482
483
484
485
486
487
488
489
490
491
492
493
494
495
496
497
498
499
500
501
502
503
504
505
506
507
508
509
510
511
512
513
514
515
516
517
518
519
520
521
522
523
524
525
526
527
528
529
530
531
532
533
534
535
536
537
538
539
540
541
542
543
544
545
546
547
548
549
550
551
552
553
554
555
556
557
558
559
560
561
562
563
564
565
566
567
568
569
570
571
572
573
574
575
576
577
578
579
580
581
582
583
584
585
586
587
588
589
590
591
592
593
594
595
596
597
598
599
600
601
602
603
604
605
606
607
608
609
610
611
612
613
614
615
616
617
618
619
620
621
622
623
624
625
626
627
628
629
630
631
632
633
634
635
636
637
638
639
640
641
642
643
644
645
646
647
648
649
650
651
652
653
654
655
656
657
658
659
660
661
662
663
664
665
666
667
668
669
670
671
672
673
674
675
676
677
678
679
680
681
682
683
684
685
686
687
688
689
690
691
692
693
694
695
696
697
698
699
700
701
702
703
704
705
706
707
708
709
710
711
712
713
714
715
716
717
718
719
720
721
722
723
724
725
726
727
728
729
730
731
732
733
734
735
736
737
738
739
740
741
742
743
744
745
746
747
748
749
750
751
752
753
754
755
756
757
758
759
760
761
762
763
764
765
766
767
768
769
770
771
772
773
774
775
776
777
778
779
780
781
782
783
784
785
786
787
788
789
790
791
792
793
794
795
796
797
798
799
800
801
802
803
804
805
806
807
808
809
810
811
812
813
814
815
816
817
818
819
820
821
822
823
824
825
826
827
828
829
830
831
832
833
834
835
836
837
838
839
840
841
842
843
844
845
846
847
848
849
850
851
852
853
854
855
856
857
858
859
860
861
862
863
864
865
866
867
868
869
870
871
872
873
874
875
876
877
878
879
880
881
882
883
884
885
886
887
888
889
890
891
892
893
894
895
896
897
898
899
900
901
902
903
904
905
906
907
908
909
910
911
912
913
914
915
916
917
918
919
920
921
922
923
924
925
926
927
928
929
930
931
932
933
934
935
936
937
938
939
940
941
942
943
944
945
946
947
948
949
950
951
952
953
954
955
956
957
958
959
960
961
962
963
964
965
966
967
968
969
970
971
972
973
974
975
976
977
978
979
980
981
982
983
984
985
986
987
988
989
990
991
992
993
994
995
996
997
998
999
1000

2.2 Chemicals

All the materials necessary for cell culture were purchased from Lonza (Lonza Sales AG, Verviers, Belgium). The ICG dye was purchased from MP Biomedicals (Santa Ana, CA, USA), whereas all other chemicals from Sigma Chemical Co. (St Louis, MO, USA) and were used as received.

2.3 MSC culture

MSCs were isolated from the bone marrow of male C57BL/6J mice (age: 7-9 weeks, weight: 22-28 g). Briefly, femurs and tibias were excised, and flushed with RPMI w/o Red Phenol supplemented with 10% FBS to harvest the bone marrow cells, which were then cultured into Minimal Essential Medium Eagle Alpha Modification supplemented with penicillin (100 U/ml), streptomycin (100 $\mu\text{g}/\text{ml}$), FBS (10%) and glutamine (2 mM). After 4 days, the MSCs were selected on the basis of their adherence to plastic, before they underwent a magnetic immune cell sorting with Microbeads conjugated to monoclonal rat antimouse/human CD11b antibody (Miltenyi Biotec GmbH, Bergish Gladbach, Germany) at day 10 to further remove CD11b⁺ granulocytic cells.

2.4 Cell labeling protocol

The ICG-labeling solution was prepared by completely dissolving the dye powder into Dimethyl Sulfoxide (DMSO), before adding the FBS-free culture medium (the v/v of DMSO/medium was 1:6). A final ICG concentration of 0.25 mg/ml was used in all experiments. MSCs were detached from flasks, added with the pre-warmed ICG-labeling solution, and left at 37°C for variable time ranges (ranging from 2 minutes to 6 hours). After labeling, the excess of dye was removed by washing the cells three times with Phosphate Buffered Saline (PBS).

2.5 Cell viability and proliferation rate

Cell viability was estimated by using the Trypan Blue exclusion assay. The reported viability percentage value represents the average ratio between the number of viable

1
2 cells N_v and the total number of cells N_{tot} ($N_v/N_{tot} \times 100$).
3 Similarly, for proliferation tests the cells were seeded after
4 labeling and maintained in standard culture conditions for
5 different time ranges (up to 8 days), before being counted.
6 The proliferation ability is expressed as the average ratio
7 between the number of cells at each time point N_t and the
8 number of cells present at the beginning of the experiment
9 N_0 (N_t/N_0).

10 2.6 Flow cytometry

11 Cells were resuspended in PBS supplemented with 0.1%
12 BSA and incubated with fluorochrome-conjugated
13 monoclonal antibodies (mAb) for 30 min at 4°C. The
14 following mAbs (final dilution: 1/20) were used: anti-
15 CD29-(PE), anti-CD44-APC, anti-CD11b-FITC, anti-
16 CD90-(PE) (BD Bioscience Pharmingen, San Jose, CA,
17 USA), anti-Sca1-(PE) (Cedarlane, Burlington, Ontario,
18 Canada), and anti-CD105-PE (MACS Miltenyi Biotec,
19 San Diego, CA, USA). The fluorescence was measured
20 using the FACS Calibur flow cytometer equipped with
21 CellQuest software (BD Biosciences).

22 2.7 Optical absorbance and emission of labeled 23 cells

24 The cell uptake of ICG was estimated by fluorimetry.
25 Briefly, the labeling incubation was carried on for 60
26 minutes. After exhaustive washing, cells were counted,
27 suspended at the final concentration of 3.0×10^6 cells/ml in
28 PBS, sonicated by using a Bandelin Sonoplus Sonicator
29 (20kHz, 20 W, 30s), and analysed by a FluoroMax-4
30 Spectrofluorometer (Horiba Scientific, Edison New
31 Jersey, USA) equipped with the driving software
32 FluorEssence™ for Windows. The number of ICG
33 molecules internalized by the single cell was estimated on
34 the basis of the signal intensity values measured at 803 nm
35 and reported on the calibration curves which were
36 previously obtained. The experiment was repeated four
37 times.

38 2.8 Cell transplantation

39 Healthy male C57BL/6J mice (weight: 25-28 g, age: 10-
40 12 weeks) were anaesthetized, and their hindlimbs were
41 shaved. After labeling, 3.0×10^5 MSCs were collected,
42 suspended in 100 μ L of PBS, and injected into the
43 gastrocnemius muscle of the right hindlimb by using a 1-
44 ml syringe with a 25-G \times 5/8-in needle (BD, Franklin
45 Lakes, NJ). Equivalent numbers of control unlabeled cells
46 were transplanted into the left hindlimb.

47 2.9 Combined ultrasound and photoacoustic 48 (US/PA) imaging

49 PAI was performed by using a VisualSonics Vevo 2100
50 LAZR Imaging Station (VisualSonics, Inc., Toronto,
51 Canada) equipped with a LZ250 transducer operating at
52 21 MHz frequency that incorporates photoacoustic
53 imaging into high-resolution ultrasound imaging. Cell
54 suspensions were loaded onto a custom-made phantom for

photoacoustic *in vitro* acquisitions, equipped with
stretched plastic capillaries to contain liquid samples,
further surrounded by solidified agarose gel to provide
favourable interface for US propagation. The
photoacoustic transducer was set perpendicularly to the
capillaries, such that images reproducing their axial
sections were acquired. The PA signal intensity was
recorded by switching the excitation over the wavelength
range included between 680 and 960 nm, and graphed as
a spectrum. The normalized photoacoustic spectrum for
each sample was obtained by subtracting the contribution
of the blank (either PBS or unlabeled cells suspended in
PBS) at each wavelength λ , as follows:

$$NPA_{\lambda} = PA_{sample \lambda} - PA_{ctrl \lambda}$$

where NPA is the normalized photoacoustic signal,
 PA_{sample} and PA_{ctrl} stand for the photoacoustic intensity
at each wavelength λ of each *sample* or *ctrl*, respectively.
Each experiment was repeated in triplicate.

For *in vivo* imaging, anaesthetized animals were
accurately shaved on their hindlimbs. Combined US/PA
images were obtained by overlaying photoacoustic
intensities on the ultrasound images with user-defined
grayscale thresholds. PA intensity values measured on the
transplantation site of labeled cells (right hindlimb) were
normalized with respect to the signal recorded on the same
anatomical region of the left hindlimb after the injection
of the control unlabeled cells, as reported in the following
formula:

$$PA_{Enh} = \frac{PA_{right} - PA_{left}}{PA_{left}}$$

where PA_{right} and PA_{left} represent the photoacoustic
signal measured in the right and left hindlimb at different
wavelengths included between 680 and 960 nm,
respectively. Spectra recorded before the cell
transplantation (Pre-Injection) were provided to show the
local endogenous photoacoustic baseline of the muscular
tissue. The signal intensity quantification was carried out
at fixed excitation wavelength (810 nm).

51 2.10 Optical imaging

52 The photon emission from the labeled cells was measured
53 *in vitro* on the Pearl Imager (LI-COR Biosciences,
54 Lincoln, NE) with preset near infrared excitation (710-
55 760 nm) and emission (810-875 nm) pass band filters to
56 evaluate the ICG signal. The *in vivo* studies were carried
57 out on the IVIS Spectrum Whole Animal Imaging System
58 (Perkin Elmer Inc., Waltham, Massachusetts, USA). The
59 animals were irradiated with filter light of wavelength 745
60 nm, and an image of emission intensity was collected at
61 840 nm (field of view = 14 cm, fstop = 2, binning =
62 medium, exposure time = auto). As for the photoacoustic
63 experiments, the fluorescence-imaging signal intensity
64 values were measured on the transplantation site of
65 labeled cells (right hindlimb), and normalized with respect

1
2 to control unlabeled cells (left hindlimb). The
3 Fluorescence Imaging Enhancement ($FLEnh$) was
4 expressed as:

$$5 \quad FLEnh = \frac{FLE_{right} - FLE_{left}}{FLE_{left}}$$

6
7
8 where FLE_{right} and FLE_{left} represent the fluorescence
9 intensity measured in the right and left hindlimb,
10 respectively.
11

12 2.11 Statistical analysis

13 All data were presented as Mean Values \pm Standard Error
14 of the Mean (MV \pm SE). Statistical significance was
15 determined by either the unpaired Student *t*-test or the
16 Analysis of the Variance (ANOVA) test, as indicated in
17 each graph. The *p*-values ≤ 0.05 and 0.01 were marked as
18 * and **, respectively.
19
20
21

22 3. Results

23 3.1 Optimization of the cell labeling procedure

24 The labeling procedure was performed by detaching and
25 incubating MSCs with ICG-containing medium at 37°C
26 (**Figure 1A**). According to previous studies,[31] a final
27 ICG concentration of 0.25 mg/mL was selected to perform
28 all labeling experiments, and the procedure was optimized
29 by subjecting the MSCs to different incubation times. For
30 the longest incubation times, an inverse proportionality
31 between cell viability and duration of the labeling was
32 observed (**Figure 1B**), with a significant (*t*-test *p*-value \leq
33 0.01) viability reduction specifically induced by
34 incubations lasting 3 and 6 h (18.9% and 24.3%,
35 respectively). In these conditions, cells also showed
36 impaired proliferation ability (**Figure 1C**): a decreased
37 fraction of viable cells was found at different time points
38 after labeling, culminating at day 8 when the proliferation
39 rate for both the conditions was dramatically reduced
40 (33.3 % and 40.7 %, respectively, ANOVA *p*-value \leq
41 0.01) with respect to control cells. In the other tested
42 labeling times, no relevant changes in viability were
43 detected, therefore suggesting that an incubation time of 1
44 h may be considered optimal for safe labeling in
45 maximum loading conditions. The molecular
46 internalization rate after 1h incubation was therefore
47 determined by estimating the ICG content per cell via
48 fluorimetric assay directly on labeled cell suspensions,
49 such that an uptake of $(1.7 \pm 0.4) \times 10^{10}$ molecules/cell was
50 calculated, corresponding to an internalization efficiency
51 of approximately 0.9 ± 0.2 %. Finally, as observed by flow
52 cytometry, the 1 h exposure to ICG did not induce any
53 alteration in the expression profile of cell surface markers
54
55
56
57
58
59

(**Figure 1D**), revealing a complete retention of the MSC
phenotype.

3.2 In vitro imaging

The photoacoustic and fluorescent properties of ICG were
preliminary investigated with the respective imaging
systems (**Figure 2 and 3**). The photoacoustic signal of
differently concentrated ICG aqueous solutions in a
submillimolar range was acquired by tuning the excitation
wavelength from 680 to 970 nm in order to study the PA
sensitivity and spectrum *in vitro* (**Figure 2A and B**). The
intensity at the initial phase of the spectral profile
increased with the dye concentration, and even if a
photoacoustic detection limit of 25 μ M was identified
elsewhere on a different PA imaging station,[32] in our
setup we were able to clearly detect the molecule at a
concentration of 15 μ M (**Figure 2A**) according to what
was already reported by others using the same
instrument.[33] The PA signal tended to drop as the
excitation was swept to high wavelengths (> 830 nm) and
became eventually negligible at 950 nm, even at the
highest concentration tested (*i.e.*, 1 mM). However, a
certain concentration-dependent variability in the spectral
shapes was observed: whereas the 1 mM ICG presented a
sharp peak centered at 710 nm, in diluted solutions the
molecule displayed a more flattened spectral profile
characterized by the presence of two peaks. Further
lowering the concentration, a more defined peak at 800
nm appeared. Since this observation approximately
matched the finding of a recurrent main peak at around
810 nm reported by Park *et al.*[32], we selected this
excitation wavelength as reference value to perform the
signal quantification and acquire representative images. In
order to test the effects of a possible interaction between
ICG and cellular components, samples containing the dye
at variable concentrations and a fixed number (3.0×10^5) of
MSCs were analyzed immediately after mixing (**Figure**
2C and D). Interestingly, in the presence of cells the PA
signal intensity at the spectral initial phase increased for
almost all the samples (*ca.* 2-fold increase at 15 and 100
 μ M and even 3-fold at 1 mM ICG). Although some
variations in the spectral shape were observed at the
highest investigated ICG concentration, for the
micromolar ICG the main peak wavelength shifted within
the 800-820 nm interval, confirming that the PA
excitation may be performed at maximum efficacy in this
range. Finally, also cells labeled with the ICG according
to our optimized protocol were analyzed (**Figures 2E and**
2F). This experiment was carried out by resuspending
 3.0×10^5 ICG-labeled MSCs in decreasing PBS volumes,
thus varying both the cell density and the final volume of
the suspension. We assumed that the ICG amount uptaken
by the cells during the labeling procedure led to a final dye

1
2 concentration in the μM range, as it was previously
3 determined by fluorimetry. Indeed, the spectral shape of
4 the labeled MSCs recapitulated the one observed in the
5 presence of the micromolar dye, being characterized by a
6 main peak at about 820 nm. Very interestingly, the ICG
7 internalized within cells produced a strong PA signal,
8 which increased of *ca.* 25 % and 85 % as compared to the
9 100 μM ICG sample with and without cells, respectively.
10 Indeed, the PA signal intensity was comparable to that of
11 the 1 mM ICG mixed with cells (**Figure 2G**), thus
12 indicating that an optoacoustic enhancement can likely be
13 obtained through the intracellular compartmentalization
14 of the dye. Interestingly, only subtle variations in the PA
15 signal intensity were found when labeled cells were
16 differently concentrated into PBS (**Figures 2E and 2F**),
17 possibly suggesting that phenomena of liquid reabsorption
18 that commonly follow the inoculation of cells into tissue
19 might only induce minimal effects on the signal intensity.
20 All the samples were also analyzed in terms of NIRF
21 intensity, as expressed in Average Radiant Efficiency
22 (**Figure 3**). For both ICG aqueous solutions and ICG-cell
23 mix, the concentration-dependent initial increase of the
24 fluorescence peaked at 50 μM , and was followed by a fast
25 decrease (**Figures 3A and 3B**) in accordance to previous
26 studies indicating that dye concentrations exceeding 200
27 μM are not detectable due to quenching phenomena.[32]
28 The fluorescent behaviour of ICG only differed at 100
29 μM , where a slightly reduced emission occurred in the
30 presence of cells. Interestingly, in the suspensions of ICG-
31 labeled cells (**Figures 3C and 3D**) the NIRF contrast
32 enhancement calculated over the baseline (unlabelled
33 cells) at the lowest and highest cell concentrations
34 (namely 3000 and 15000 cell/ μl) corresponded to +300
35 and 220%, respectively, therefore showing a mild
36 reduction of the fluorescent emission towards high cell
37 densities. Nonetheless, these signal variations were
38 recorded in the same magnitude range of intensity,
39 reflecting a relatively limited potential of the cell density
40 to affect the NIRF emission. Additionally, we also
41 demonstrated that both the photoacoustic and fluorescent
42 emissions increased with the incubation time (**Figure**
43 **S1A**), but whereas the PA signal amplitudes recorded on
44 suspensions of cells labeled for 2 minutes were not
45 distinguishable from the baseline, the fluorescent signal
46 could be detected in all the tested conditions (**Figure**
47 **S1B and C**). Finally, the PA and NIRF signal intensity from
48 cells incubated for 1 h was significantly (ANOVA, *p*-
49 value < 0.01) higher with respect to all other conditions
50 (**Figures S1A and S1B**), confirming this incubation time
51 as optimal for imaging efficiency.

52 3.3 *In vivo* imaging

The *in vivo* study was carried out by locally transplanting
3.0 $\times 10^5$ ICG-labeled MSCs into the gastrocnemius
muscle of the right hindlimb of healthy C57BL/6J mice.
The site of cell deposition was clearly detected by US
imaging (B-mode, 21 MHz), as a consequence of the
change in the acoustic impedance determined by the dense
inoculated cell mass (**Figure 4A**). The PA signal intensity
generated by the ICG-MSCs was normalized over the
local endogenous baseline recorded in the left hindlimb of
the animal where the transplantation of control unlabeled
cells was performed (representative pictures in **Figure**
4**B**) and expressed as photoacoustic enhancement (PA_{Enh} ,
see Experimental for details). The PA_{Enh} was measured
over the entire range of excitation wavelengths
immediately after cell transplantation, then monitored
over time, and reported as PA spectrum in **Figure 4C**.
Interestingly, immediately and 4 hours post-injection, the
maximum peak recorded in the photoacoustic spectra was
shifted towards high excitation wavelength values (890
and 920 nm, respectively), whereas from day 1 to day 4,
the spectral shape reproduced the one observed *in vitro*
with a maximum enhancement centered at around 810 nm
(**Figures 4D and 4E**). Finally, the normalized PA spectra
acquired 7 days post injection presented a flat shape
without any discernable peak. **Figure 4F** displays the
time-dependent variation of the signal as quantified at
both 810 nm and the wavelength corresponding to the
maximum peak recorded in each spectrum, whereas
Figure 4G shows representative images of the time
evolution of PA emission in regions of interest (ROIs) at
tissue depth comprised between 1 and 5 mm. Moreover,
the entire procedure of cell injection was caught on video
(**Movie S1**) and 3D reconstructions of the ICG-MSC
engraftment in the right calf were elaborated using
Vevo@Lab 1.7.2 software (**Figure S2 and Movies S2 and**
5**S3**). Immediately after cell transplantation, a considerably
high PA amplitude was measured in the inoculation site
(**Figures 4C and 4F**). By summing up the PA signal areas
as calculated on bidimensional ROIs drawn in consecutive
images over the entire muscular region, an engraftment
volume of around 70 mm^3 was estimated, which is
consistent to the injection procedure of a 100 μl cell
suspension. Then, a progressive time-dependent decrease
in the signal intensity occurred, revealing that the labeled
MSCs could be optoacoustically detected until 3 days
before the loss of the ICG-related signal and the
prevalence of unspecific signal components let the
contrast enhancement become almost negligible (**Figure**
4**F**). After each PA acquisition, the mice underwent NIRF
imaging in order to assess the fluorescent contrast
enhancement (FLI_{Enh}) produced by the transplanted cells
(**Figures 5A and 5B**). Interestingly, before progressively
fading over days (likely due to the dye degradation and
washout), the FLI_{Enh} values followed an initial rising trend
during the first 24 h after the engraftment deposition. The
coincident observation of extremely high PA amplitudes
(**Figures 4C and 4F**) suggests that at early time points the
strong intermolecular interactions among ICG molecules

1
2 contribute to the quenching of the fluorescence, but
3 results at the same time into an increase of the
4 photoacoustic effect, due to photothermal conversion by
5 nonradiative decay.[33] Finally, the time limit for the
6 engraftment detection by NIRF matched that one enabled
7 by the photoacoustic decay (namely, 3 days *p.i.*). Similar
8 conclusions derived from an additional series of
9 experiments performed by transplanting a higher cell
10 number (1.0×10^6 cells, **Figures S3 and S4**). As expected,
11 a more intense and persistent contrast enhancement was
12 obtained in both techniques, pushing further the detection
13 limit day. In particular, a photoacoustic signal was still
14 detected 7 days after transplantation, which truly
15 corresponded to sparse residual ICG-labeled MSCs, as
16 proved by histological examination in the inoculation site
17 (**Figure S5**).

20 4. Discussion

21
22
23 According to pre-clinical and clinical research conducted
24 thus far, cell imaging should be assimilated into more
25 studies focused on the use of cell-transplantation for
26 therapeutic purposes.[30] In fact, the imaging techniques
27 that facilitate the unambiguous *in vivo* identification and
28 characterization of the cell engraftments are invaluable for
29 assessing the survival and the functional integration of
30 exogenous cells, and for optimizing the delivery as well.
31 The present work aimed at addressing these issues by
32 merging the advantages offered by the well-known and
33 safe profile of ICG with the emergent technique of PAI.
34 For the first time the potential application of the free ICG
35 as cell labeling agent and photoacoustic tracer was
36 explored. As already done by Uthaman *et al.*,[34] the PA
37 visualization of the cell engraftment was paralleled by
38 NIRF acquisition in order to perform a comparative study
39 of the two imaging modalities. Despite the minor toxicity
40 and the related advantages for *in vivo* applications, ICG
41 exhibits very complex optical properties. Besides being
42 largely dependent on the solvent, concentration and
43 interaction with other molecules,[22,23,26] the absorption
44 and emission spectra are also broad and overlapping, thus
45 causing a significant re-absorption of the fluorescence by
46 the dye itself. Moreover, as extensively reviewed by
47 Desmettre *et al.*,[22] the molecule can be affected by
48 photodegradation and, at high concentrations, its effective
49 absorption does not linearly increase with concentration
50 due to the dye aggregation. More in details, because of its
51 amphiphilic properties, ICG is mainly present in the
52 monomer form at concentrations below 5 μM , whereas
53 over 100 μM the oligomer form prevails. The ICG
54 oligomers display a weaker fluorescence yield, affecting
55 the absorbance spectrum. Thus, a dramatic boost of the
56 ICG concentration is not expected to result in a substantial
57 signal enhancement, as we also noticed by both PA and
58 NIRF imaging. Alternatively, in order to increase the
59 quantum yield and the fluorescence intensity of the

carbocyanine dye, a stable interaction with phospholipids
could be envisaged.[35] Such crucial aspect has been
extensively exploited for the preparation of several ICG-
loaded nanosystems thus far,[35-36] and coherently, in
our experiments the simple mixture of ICG with cells
produced a marked increase in the PA intensity values,
which could be possibly ascribed also to its interaction
with cell membranes. On the other hand, the additional PA
increase we observed in the cells after incubation with the
dye could be hypothetically justified also by a mechanism
of oligomer formation occurring as a consequence of the
intracellular compartmentalization. Importantly, in the
present study a cell labeling procedure advantageous in
terms of both cellular uptake and generated imaging signal
was proposed. Remarkably, in these conditions the
exposure to the contrast agent did not produce any
relevant alteration in the cell profile, suggesting that ICG-
labeled MSCs may retain their therapeutic efficacy.
Finally, when it comes to *in vivo* use of the ICG, the
results interpretation is further complicated by the
intricacy of molecular interactions with the various
components of the biological environment.[22,34] Here,
the photoacoustic behaviour of the dye was investigated
in complex circumstances involving concentration-
dependent effects, internalization by cells, interactions
with cell components, and deposition into living tissues.
Since several common applicative scenarios require the
transplantation of hundreds of thousands of MSCs,[37-38]
we representatively performed our experiments by
labeling and monitoring 3.0×10^5 cells to verify whether
this procedure could be of effective utility and practical
interest. Our *in vivo* proof of principle productively
demonstrated that cells can be visualized into living tissue
by both PAI and NIRF over few days after transplantation.
Though the ICG labeling enables the longitudinal
monitoring of the engrafted cells, the observation times
are shorter than for the PA-detectable nano-objects
reported in literature,[17] most likely due to the faster
release of the dye from cells, as already observed by
Boddington *et al.*[29] However, also the risks connected
to the long-term tissue accumulation of exogenous
compounds have to be carefully considered, especially in
proximity of delicate therapeutic cell grafts. Additionally,
we established that a reliable quantification of the
photoacoustic signal at 810 nm can be performed only
starting from 24 h after transplantation, since the prior
time points are affected by a bathochromic shift of the
ICG signal, possibly related to the extremely high local
concentration of the dye. As in the same time window we
detected the co-presence of PA peaks centred at around
900 nm and reduced NIRF signal, we argued that the two
phenomena may be correlated by an exchange of the
emission mechanism (*i.e.* from radiative to acoustic),
likely depending on the ICG concentration. However, in
general terms, it also has to be taken into account that
immediately or shortly after surgery, tissues frequently
display imaging artefacts caused by haemorrhages and/or
micro air bubbles deposition, which make it arduous to

1
2 define the real source of the observed contrast, thus
3 preventing an accurate quantification in early monitoring.
4 This aspect becomes more relevant when the local
5 transplantation is carried out in the absence of specific cell
6 vehicles (like hydrogels), such that the injection procedure
7 likely introduces air into tissue along the needle path.[39]
8 Therefore, we conclude that the optimal imaging window
9 offered by the present protocol corresponds to a time
10 range comprised between 1 and 3 days post-
11 transplantation, which could ideally turn out to be helpful
12 in prospective clinical or pre-clinical applications to: (i)
13 ascertain the successful outcome of surgical cell
14 deposition, (ii) describe the extension and aspect of the
15 engraftment, and (iii) follow the cell migration in
16 relatively superficial anatomical areas. Finally, we
17 demonstrated that NIRF imaging substantially
18 recapitulated and validated the information obtained by
19 PAI, thus highlighting the pivotal role of the dual-
20 modality approach in strengthening the reliability and
21 clinical utility of ICG-guided MSC imaging. In the past
22 decade, researchers have been tracking transplanted cells
23 in real-time *in vivo* mainly by Magnetic Resonance
24 Imaging (MRI), Positron emission Tomography (PET),
25 Single Photon Emission Tomography (SPECT), and
26 Optical Imaging, facing crucial issues in regard to image
27 acquisition time, method sensitivity, radiation-related
28 damage, short half-life of radioisotopes, genetic
29 manipulation to introduce reporter genes, and three
30 dimensional anatomical imaging capability.[5-11,39] The
31 high spatial resolution integrated with elevated sensitivity
32 and moderate tissue penetration depth, the FDA-approved
33 tracer and the fast image acquisition make of the herein
34 proposed protocol an attractive option to further develop
35 the techniques of direct stem cell labeling towards the
36 clinical dimension, by satisfying almost all the ideal
37 translational requirements.[40]

5. Conclusion

38
39
40
41
42 In summary, the ICG was successfully used as PA-NIRF
43 dual-mode contrast agent to label, visualize, and monitor
44 MSCs both *in vitro* and *in vivo*. Proper cell labeling
45 conditions were selected such that the cell uptake was
46 maximized, and cell viability, proliferation, and
47 phenotypic features were preserved. Since the number of
48 MSCs involved in several experimental circumstances is
49 usually either similar or higher than that used here,[35-36]
50 we conclude that in a forward-looking vision this
51 technique retains a considerable potential for
52 transplantation-focused research and therapy by providing
53 the *in vivo* cell fate surveillance with safety, real time
54 content, good endogenous contrast among soft tissues and
55 improved spatial resolution.
56
57
58
59

Supporting Information

Additional supporting information may be found in the
online version of this article at the publisher's website.

Acknowledgements Dr Giovanni Valbusa (Ephoran),
Lorenzo Ariotti (Bracco Imaging Spa), and Dr Marta Tapparo
(University of Turin) are gratefully acknowledged for their
valuable contribution to fluorescence microscopy imaging and
histological examination. FUV is gratefully acknowledged.

Author biographies please see **Supporting
Information online.**

References

1. E. Buzhor, L. Leshansky, J. Blumenthal, H. Barash, D. Warshawsky, Y. Mazor, and R. Shtrichman, *Regen Med* **9**, 649-672 (2014).
2. X. Wei, X. Yang, Z. P. Han, F. F. Qu, L. Shao, and Y. F. Shi, *Acta Pharmacol Sin* **34**, 747-754 (2013).
3. M. Das, I. B. Sundell, and P. S. Koka, *J Stem Cells* **8**, 1-16 (2013).
4. C. A. Herberts, M. S. Kwa, and H. P. Hermsen, *J Transl Med* **9**, 29 (2011).
5. A. K. Srivastava and J. W. Bulte, *Stem Cell Rev* **10**, 127-144 (2014).
6. M. E. Kupfer and B. M. Ogle, *Biotechnol J* **10**, 1515-1528 (2015).
7. Y. Zhao, A. J. Bower, B. W. Graf, M. D. Boppart, and S. A. Boppart, *Methods Mol Biol* **1052**, 57-76 (2013).
8. E. J. Sutton, T. D. Henning, B. J. Pichler, C. Bremer, and H. E. Daldrup-Link, *Eur Radiol* **18**, 2021-2032 (2008).
9. Z. Yang, Q. Zeng, Z. Ma, Y. Wang, and X. Xu, *J Vis Exp* **31**, 10.3791/1388 (2009).
10. J. E. Kim, S. Kalimuthu, and B. C. Ahn, *Nucl Med Mol Imaging* **49**, 3-10 (2015).
11. Y. Hakamata, T. Murakami, and E. Kobayashi, *Transplantation* **81**, 1179-1184 (2006).
12. R. Bouchard, O. Sahin, and S. S. Emelianov, *IEEE Trans Ultrason Ferroelectr Freq Control* **61**, 450-466 (2014).
13. J. Kim, D. Lee, U. Jung, and C. Kim, *Ultrasonography* **34**, 88-97 (2015).
14. L. Cunha, I. Horvath, S. Ferreira, J. Lemos, P. Costa, D. Vieira, D. S. Veres, K. Szigeti, T. Summavielle, D. Máthé, and L. F. Metello, *Mol Diagn Ther* **18**, 153-173 (2014).
15. X. Yang, E. W. Stein, S. Ashkenazi, and L. V. Wang, *Wiley Interdiscip Rev Nanomed Nanobiotechnol* **1**, 360-368 (2009).
16. S. Manohar, C. Ungureanu, and T. G. Van Leeuwen, *Contrast Media Mol Imaging* **6**, 389-400 (2011).

- 1
2
3
4
5
6
7
8
9
10
11
12
13
14
15
16
17
18
19
20
21
22
23
24
25
26
27
28
29
30
31
32
33
34
35
36
37
38
39
40
41
42
43
44
45
46
47
48
49
50
51
52
53
54
55
56
57
58
59
60
61
62
63
64
65
17. S. Y. Nam, L. M. Ricles, L. J. Suggs, and S. Y. Emelianov, *PLoS One* **7(5):e37267**, 10.1371/journal.pone.0037267 (2012).
 18. H. Gong, R. Peng, and Z. Liu **65**, 1951-1963 (2013).
 19. A. J. Andersen, P. P. Wibroe, and S. M. Moghimi, *Adv Drug Deliv Rev* **64**, 1700-1705 (2012).
 20. Z. Krpetić, S. Anguissola, D. Garry, P. M. Kelly, and K. A. Dawson, *Adv Exp Med Biol* **811**, 135-156 (2014).
 21. S. Zackrisson, S. M. Van de Ven, and S. S. Gambhir, *Cancer Res* **74**, 979-1004 (2014).
 22. T. Desmettre, J. M. Devoisselle, and S. Mordon, *Surv Ophthalmol* **45**, 15-27 (2000).
 23. B. Yuan, N. Chen, and Q. Zhu, *J Biomed Opt* **9**, 497-503 (2004).
 24. J. T. Alander, I. Kaartinen, A. Laakso, T. Pätälä, T. Spillmann, V. V. Tuchin, M. Venermo, and P. Välisuo, *Int J Biomed Imaging* **2012:940585**, 10.1155/2012/940585 (2012).
 25. H. Abe, T. Mori, T. Umeda, M. Tanaka, Y. Kawai, T. Shimizu, H. Cho, Y. Kubota, Y. Kurumi, and T. Tani, *Surg Today* **41**, 197-202 (2011).
 26. C. Jonak, H. Skvara, R. Kunstfeld, F. Trautinger, and J. A. Schmid, *PLoS One* **6(8):e23972**, 10.1371/journal.pone.0023972 (2011).
 27. R. Alford, H. M. Simpson, J. Duberman, G. C. Hill, M. Ogawa, C. Regino, H. Kobayashi, and P. L. Choyke, *Mol Imaging* **8**, 341-354 (2009).
 28. M. Ogawa, N. Kosaka, P. L. Choyke, and H. Kobayashi, *Cancer Res* **69**, 1268-1272 (2009).
 29. S. E. Boddington, T. D. Henning, P. Jha, C. R. Schlieve, L. Mandrussow, D. DeNardo, H. S. Bernstein, C. Ritner, D. Golovko, Y. Lu, S. Zhao, and H. E. Daldrup-Link, *Cell Transplant* **19**, 55-65 (2010).
 30. V. Sabapathy, J. Mentam, P. M. Jacob, and S. Kumar, *Stem Cells Int* **10.1155:2015**, 10.1155/2015/606415 (2015).
 31. J. D. Ho, R. J. Tsai, S. N. Chen, and H. C. Chen, *Br J Ophthalmol* **88**, 556-559 (2004).
 32. S. Park, J. Kim, M. Jeon, J. Song, and C. Kim, *Sensors (Basel)* **14**, 19660-19668 (2014).
 33. G. Ferrauto, F. Carniato, E. Di Gregorio, L. Tei, M. Botta, and S. Aime, *Nanoscale* **9**, 99-103 (2017).
 34. S. Uthaman, J. S. Bom, H. S. Kim, J. V. John, H. S. Bom, S. J. Kim, J. J. Min, I. Kim, and I. K. Park, *J Biomed Mater Res B Appl Biomater* **104**, 825-34 (2016).
 35. J. C. Kraft and R. J. Y. Ho, *Biochemistry* **53**, 1275-1283 (2014).
 36. E. Portnoy, N. Vakruk, A. Bishara, M. Shmuel, S. Magdassi, J. Golenser, and S. Eyal, *Theranostics* **6**, 167-76 (2016).
 37. K. Serigano, D. Sakai, A. Hiyama, F. Tamura, M. Tanaka, and J. Mochida, *J Orthop Res* **28**, 1267-1275 (2010).
 38. K. Mareschi, D. Rustichelli, R. Calabrese, M. Gunetti, F. Sanavio, S. Castiglia, A. Risso, I. Ferrero, C. Tarella, and F. Fagioli, *Stem Cells Int* **2012:920581**, 10.1155/2012/920581 (2012).
 39. E. Bull, S. Y. Madani, R. Sheth, A. Seifalian, M. Green, and A. M. Seifalian, *Int J Nanomedicine* **9**, 1641-1653 (2014).
 40. J. V. Frangioni and R. J. Hajjar, *Circulation* **110**, 3378-3383 (2004).

Figures

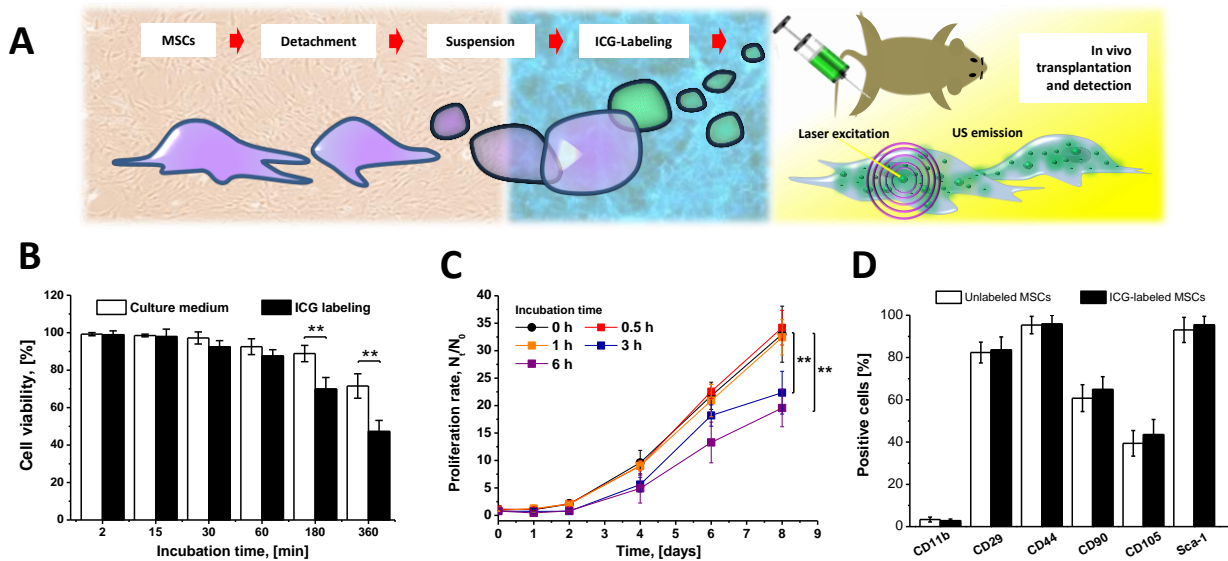


Figure 1. Cytotoxic effects induced by the ICG. (A) Schematic diagram of the adopted procedure for ICG-labeling and *in vivo* detection of MSCs. (B) Cell viability estimated on MSCs incubated with 0.25 mg/ml ICG-containing medium for different time ranges. Cells incubated with culture medium were used as control. (C) Proliferation rate of MSCs subjected to the ICG-labeling for different time ranges (0 h refers to control cells that did not undergo the labeling procedure). (D) Marker expression profiles analysed by flow cytometry showing a high conformity between ICG-labeled and unlabeled MSCs. A basic characterization of the primary murine stem cells was provided through the analysis of different surface markers defining the MSC profile (CD44⁺, CD90⁺, CD29⁺, CD105⁺, Sca-1⁺, and CD11b⁻).

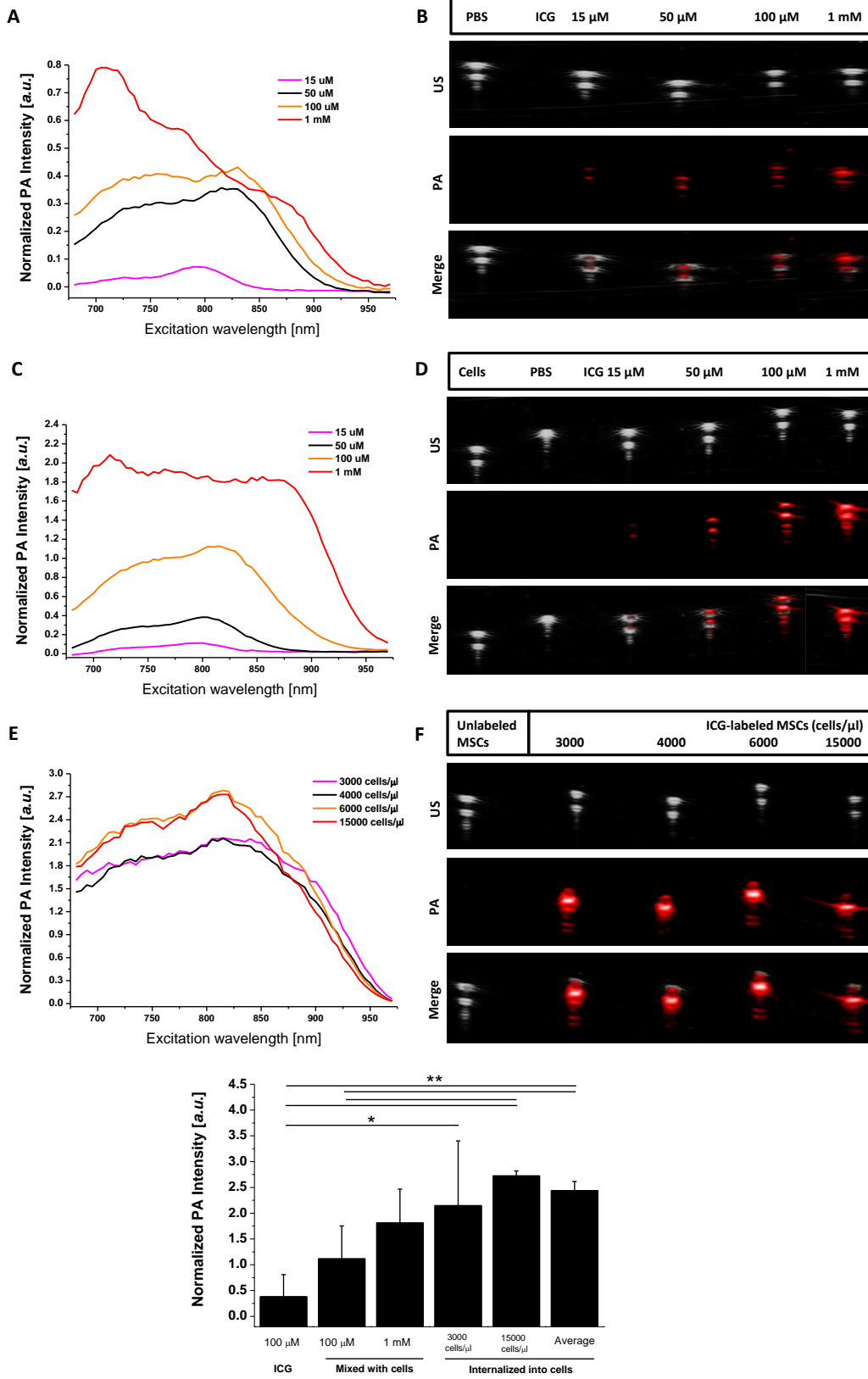


Figure 2. In vitro PA imaging of ICG. Photoacoustic spectra (A, C, and E) and representative imaging (B, D, and F) in pure photoacoustic mode (PA), ultrasounds (US) or merged imaging of: aqueous ICG solutions at different concentrations (A and B), 3.0×10^5 unlabeled MSCs resuspended in differently concentrated ICG solutions (C and D) and 3.0×10^5 ICG-labeled MSCs resuspended at different cell concentrations in PBS (E and F). (G) PA signal quantification at fixed wavelength (810 nm) of ICG in free form, in the presence of cells, and internalized into cells after labeling. ‘Average’ refers to average value of signal from all cell densities conditions. Statistical significance was determined by the unpaired Student *t*-test.

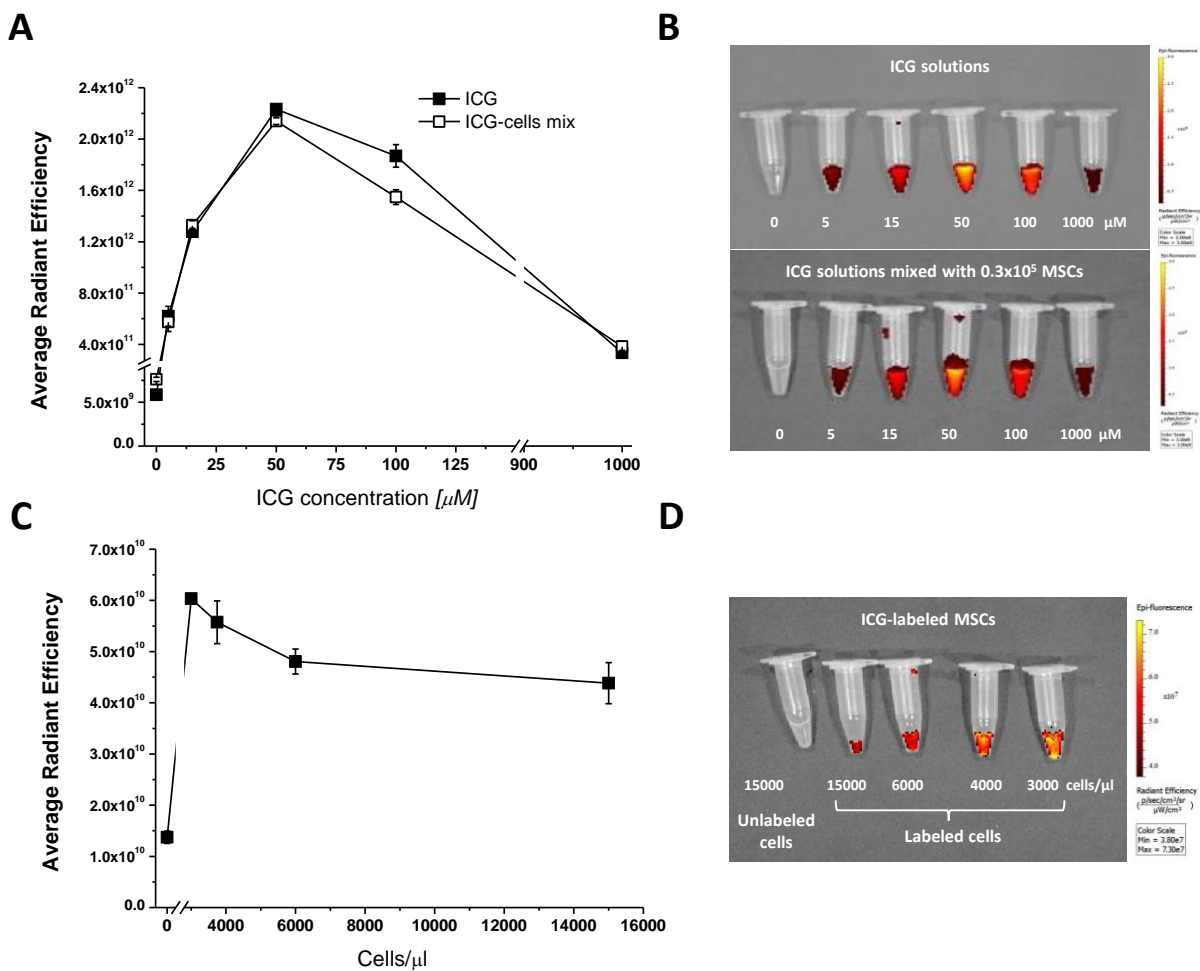


Figure 3. In vitro optical imaging of ICG. Fluorescence intensity (as expressed in average radiant efficiency) and representative imaging of aqueous ICG solutions at different concentrations either in the absence or in the presence of 3.0×10^5 unlabeled MSCs (A and B), and differently concentrated suspensions of ICG-labeled MSCs (C and D).

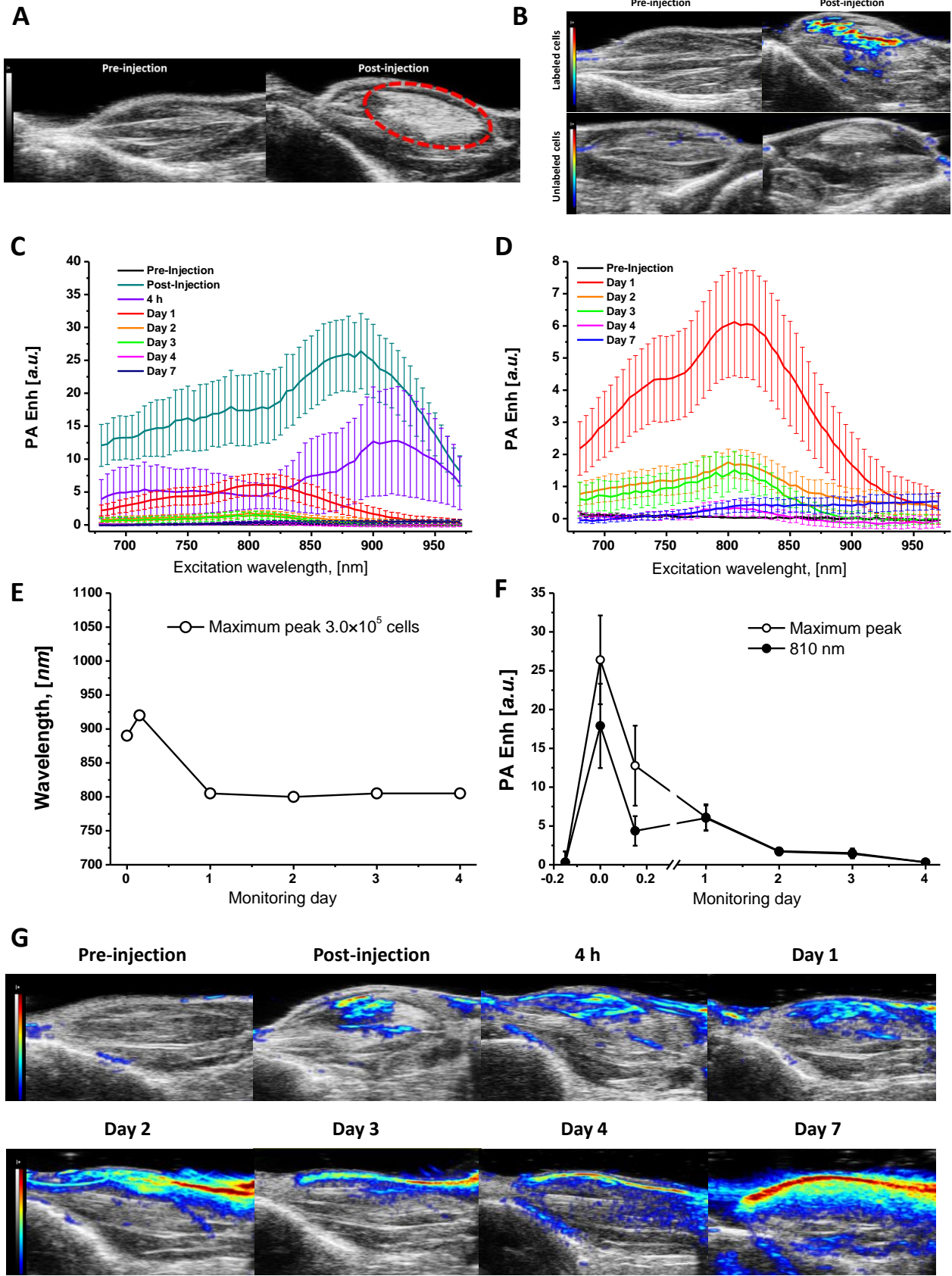


Figure 4. *In vivo* local PA Signal Intensity after cell transplantation. (A) Representative B-Mode Ultrasound imaging showing the deposition site of 3.0×10^5 unlabeled MSCs after intramuscular transplantation. (B) Representative combined Ultrasound and Photoacoustic (US/PA) images recorded at the PA excitation wavelength of 810 nm, showing the inoculation site before and after the transplantation of 3.0×10^5 ICG-labeled MSCs (right hindlimb, top), or an equivalent number of control unlabeled cells (left hindlimb, bottom). (C) Photoacoustic spectra recorded in the inoculation site at variable time ranges after cell deposition, expressed as Photoacoustic enhancement (PA Enh) over the control unlabelled cells. (D) Shape of the photoacoustic spectra recorded at time points starting from day 1. (E) Excitation wavelength of the main peak in the PA spectra during monitoring. (F) Photoacoustic contrast enhancement measured at the excitation wavelength of 810 nm and at that corresponding to the maximum spectral peak. (G) Representative PA monitoring (fixed excitation wavelength: 810 nm) of the cell engraftment over days. ROIs were drawn on the muscular region (internal area of the hindlimb), excluding the unspecific signal generated by the skin-induced reflection artefacts (tissue depth ≤ 1 mm).

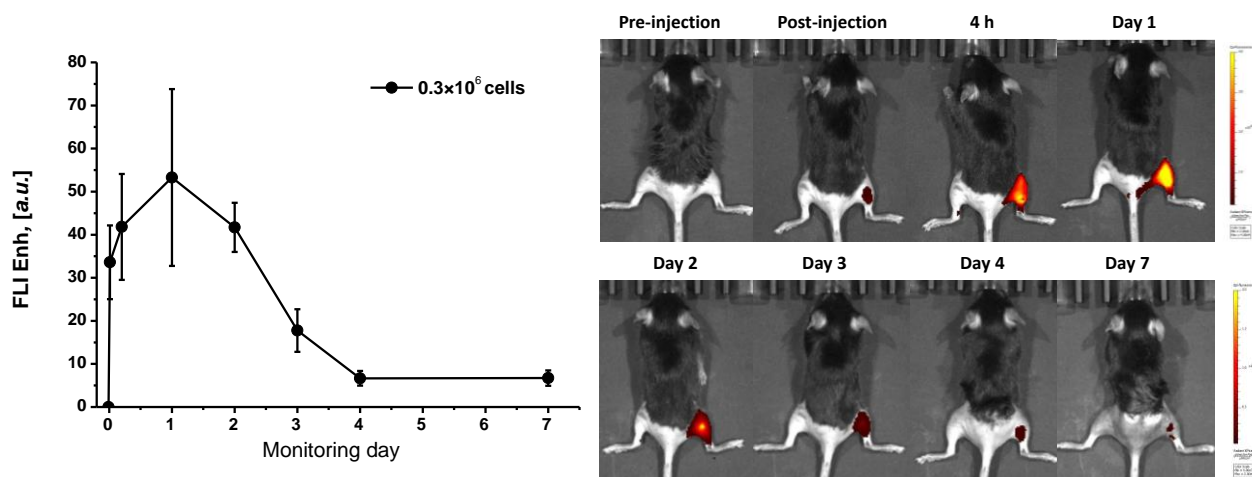
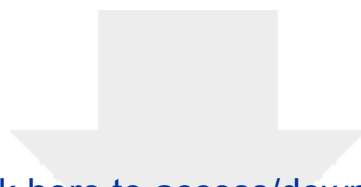


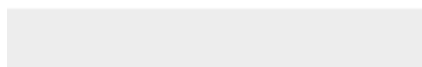
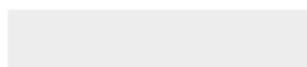
Figure 5. *In vivo* optical imaging. Fluorescence signal intensity measured after the transplantation of 3.0×10^5 ICG-labeled MSCs (excitation and emission wavelengths: 745 and 840 nm, respectively) and expressed as Fluorescence Imaging Enhancement (FLI Enh) over the control unlabeled cells (A). Representative optical images showing the time persistence of the fluorescent signal after the cell transplantation (color scale: 2.0×10^8 - 4.0×10^9 for images in the top row, 4.0×10^7 - 2.0×10^9 for images in the bottom row) (B). Calibration bars are shown.



[Click here to access/download](#)

Supporting Information

Graphical Abstract for Table of Contents.docx



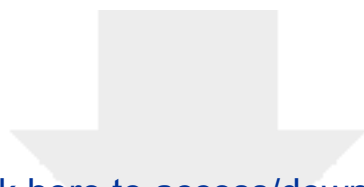


Click here to access/download
Supporting Information
Supplementary info_ICGlabeling.docx





Click here to access/download
Supporting Information
Movies.zip



Click here to access/download
Supporting Information
CV and photo of authors.docx

